 Bull. Chem. Soc. Jpn. Vol. 81, No. 8, 947–955 (2008)

Flat Resistivity in θ-Phase Charge-Transfer Salts of Selenium-Containing TMET-TTP Derivatives

Yoshimasa Bando,* Minoru Ashizawa, Tadashi Kawamoto, and Takehiko Mori

Department of Organic and Polymeric Materials, Tokyo Institute of Technology, 2-12-1 O-okayama, Meguro-ku, Tokyo 152-8552

Received January 7, 2008; E-mail: bando.y.aa@m.titech.ac.jp

Two new tetrathiapentalene (TTP)-based donor molecules have been synthesized, in which two of the four sulfur atoms of the inner TTP-skeleton of TMET-TTP (2-[4,5-bis(methylthio)-1,3-dithiol-2-ylidene]-5-(4,5-ethylenedithio-1,3-dithiol-2-ylidene)-1,3,4,6-tetrathiapentalene) are replaced by Se atoms. Four charge-transfer salts of these donors realize θ-type structures. One of the salts shows almost temperature-independent resistivity over a wide temperature range from 50 to 200 K. The calculated highest occupied molecular orbital (HOMO) is more populated on the non-Se-substituted side. This distribution is associated with the temperature-independent resistivity.

Radical-cation salts based on tetrathiafulvalene (=2-(1,3-dithiol-2-ylidene)-1,3-dithiole, TTF) derivatives have been investigated for a long time owing to their high conductivity and superconductivity. In particular, the radical-cation salts of bis(ethylenedithio)tetrathiafulvalene (BEDT-TTF) have provided a large number of two-dimensional (2D) superconductors (Scheme 1).[1] Bis-fused TTF donors with extended π-skeleton, called tetrathiapentalene (TTP) donors, have been designed to increase intermolecular interaction.[2] Although tetrakis(methylthio)-TTP (TTM-TTP, Scheme 1) has been realized half-filled metallic complexes (TTM-TTP)I_3 with a highly one-dimensional energy band,[3] bis(methylthio)ethylenedithio-TTP (TMET-TTP, Scheme 1) has afforded 2D θ-type crystals.[4]

The θ-phase has been extensively studied in θ-(BEDT-TTF)$_2$MM′(SCN)$_4$ [M = Cs, Rb and M′ = Zn, Co], and it has been proved that the metal–insulator (MI) transition temperature T_{MI} is scaled by the dihedral angle θ.[5,6] According to the universal phase diagram, T_{MI} shifts to higher temperatures with increasing θ due to the decrease of the overlap integrals.[7] The low-temperature insulating state of the representa-

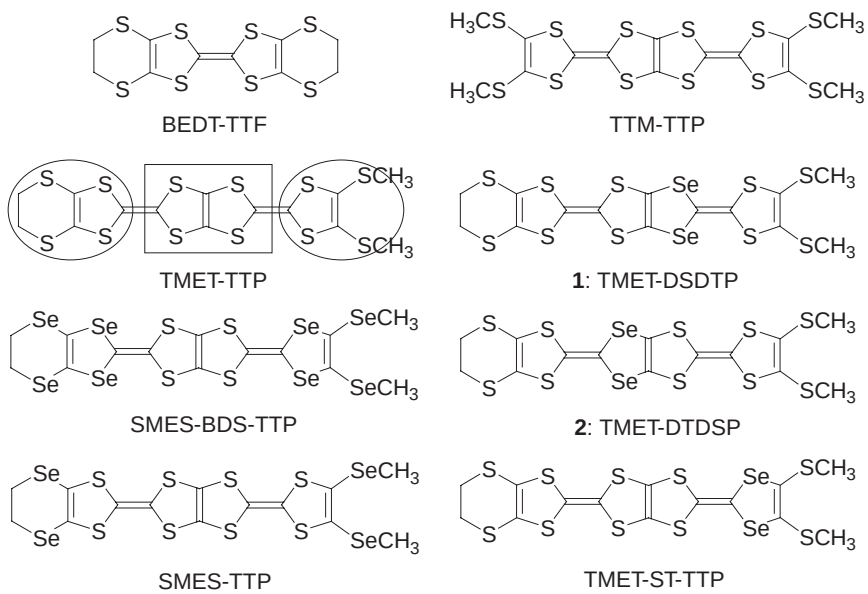

Scheme 1. Organic donor molecules (TMET-DSDTP (**1**): 5-[4,5-bis(methylthio)-1,3-dithiol-2-ylidene]-2-(4,5-ethylenedithio-1,3-dithiol-2-ylidene)-4,6-diselena-1,3-dithiapentalene, TMET-DTDSP (**2**): 2-[4,5-bis(methylthio)-1,3-dithiol-2-ylidene]-5-(4,5-ethylenedithio-1,3-dithiol-2-ylidene)-4,6-diselena-1,3-dithiapentalene, SMES-BDS-TTP: 2-[4,5-bis(methylseleno)-1,3-diselenol-2-ylidene]-5-(4,5-ethylenediseleno-1,3-diselenol-2-ylidene)-1,3,4,6-tetrathiapentalene, SMES-TTP: 2-[4,5-bis(methylseleno)-1,3-dithiol-2-ylidene]-5-(4,5-ethylenediseleno-1,3-dithiol-2-ylidene)-1,3,4,6-tetrathiapentalene, and TMET-ST-TTP: 2-[4,5-bis(methylthio)-1,3-diselenol-2-ylidene]-5-(4,5-ethylenedithio-1,3-dithiol-2-ylidene)-1,3,4,6-tetrathiapentalene).

Published on the web August 11, 2008; doi:10.1246/bcsj.81.947

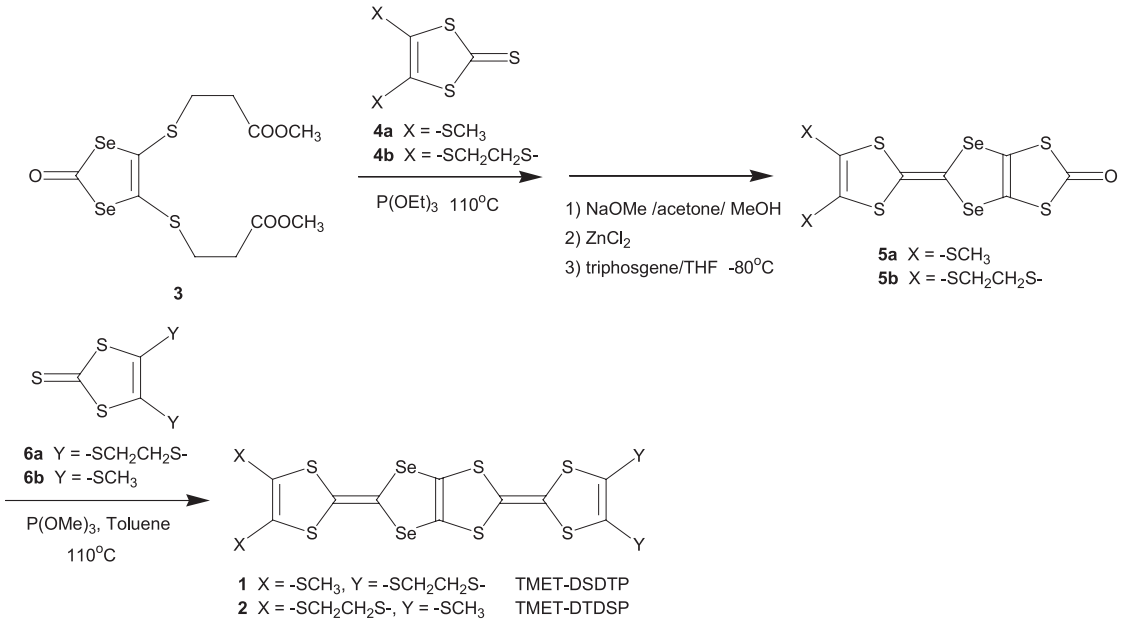

Scheme 2.

tive compound, θ-(BEDT-TTF)$_2$RbZn(SCN)$_4$, has been ascribed to the so-called "horizontal" charge order (CO) with two-fold periodicity, while the state just above T_{MI} is not a true metallic state but is a non-stripe CO state with three-fold periodicity.[8] This shows a nearly temperature independent flat resistivity, and has been verified by X-ray and NMR measurements.[8b,8c] The present paper reports a new θ-phase compound in which the flat resistivity continues in a wide temperature range from 200 to 50 K. This is achieved by Se substitution to TMET-TTP. In the TTP donors, Se substitution to the outer 1,3-dithiole rings (circled parts in Scheme 1) has been extensively carried out (TMET-ST-TTP, SMES-TTP, and SMES-BDS-TTP, in Scheme 1),[9–12] whereas Se substitution to the inner TTP-skeleton (squared part in Scheme 1) has been scarcely performed due to its preparative difficulty. So far reported is the Se substitution to the inner TTP-skeleton of TTM-TTP, where two of the four TTP sulfur atoms are replaced by Se atoms.[10] In this case, reduction of T_{MI} in a 1:5/3 triiodide salt has been reported. In the present paper, we report preparation of TMET-DSDTP (**1**) and TMET-DTDSP (**2**), crystal structures of neutral **1** and **2**, and crystal and band structures and transport properties of four radical-cation salts (PF_6 and AsF_6 salts) of **1** and **2**.

Results and Discussion

Synthesis. Scheme 2 outlines the synthesis of **1** and **2**. The compounds **3** and **5a** were prepared according to a previous report.[10] Compound **1** was prepared by the phosphite-mediated cross-coupling of **5a** and **6a**.[2,4] The compound **5b** and **2** were basically prepared by the same synthetic approaches as **5a** and **1**, but **4b** instead of **4a**, and **6b** instead of **6a** were used at the cross-coupling steps (Scheme 2).

Electrochemical Properties. The solution redox properties of the prepared donors were investigated by cyclic voltammetry. Table 1 summarizes the redox potentials together with those of the related donors. The TMET-TTP derivatives show four reversible redox couples up to 4+, corresponding to the oxidation of the four 1,3-dichalcogenole rings. The first redox potentials of **1** and **2** are slightly smaller than that of TMET-TTP but higher than that of SMES-TTP. As summarized in Figure 1, the Se substitution to the inner TTP-skeleton (3 or 4) improves the donor ability at the same level as the substitution to the outer 1,3-dithiole ring (2 or 5, TMET-ST-TTP), but in a smaller amount than the substitution to the terminal units (1 or 6, SMES-TTP) (Figure 1). Interestingly, when the outer 1,3-dithiole ring (2 or 5) and the terminal unit (1 or 6) are substituted at the same time, the donor ability is decreased (SMES-BDS-TTP).

Table 1. Redox Potentials (V)[a)]

Compounds	$E^1_{1/2}$	$E^2_{1/2}$	$E^3_{1/2}$	E^4_{ox}	$E_2 - E_1$
TMET-DSDTP (**1**)	0.54	0.78	1.02	1.20	0.24
TMET-DTDSP (**2**)	0.53	0.77	0.97	1.14	0.24
TMET-TTP	0.55	0.79	1.01	1.16	0.24
TMET-ST-TTP[12]	0.53	0.76	1.01	1.29	0.23
SMES-TTP[11]	0.50	0.77	1.16	1.31	0.27
SMES-BDS-TTP[12]	0.59	0.84	1.06	1.28	0.25

a) vs. Ag/AgCl in Bu_4PF_6/PhCN at a Pt working electrode, at room temperature, and the redox values are averages for the three scan rates of 25, 50, and 100 mV s^{-1}.

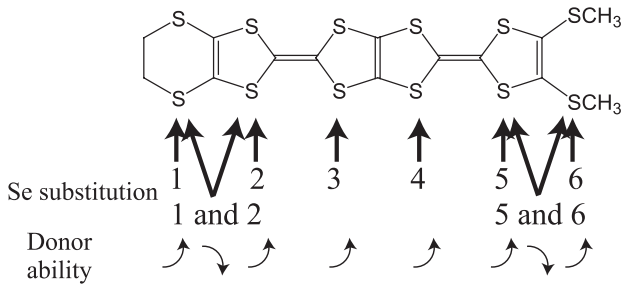

Figure 1. Selenium substitution dependence of the donor abilities of TMET-TTP.

Table 2. Crystallographic Data of the Neutral Crystals

	TMET-DSDTP (**1**)	TMET-DTDSP (**2**)
Chemical formula	$C_{14}H_{10}S_{10}Se_2$	$C_{14}H_{10}S_{10}Se_2$
Formula weight	656.75	656.75
Shape	Red plate	Red plate
Crystal system	Monoclinic	Orthorhombic
Space group	$P2_1$	$P2_12_12_1$
a/Å	14.708(3)	12.783(3)
b/Å	9.8284(9)	9.211(4)
c/Å	7.6975(7)	18.462(7)
β/°	91.23(1)	
V/Å^3	1112.5(2)	2174(1)
Z	2	4
D_{calcd}/g cm^{-3}	1.96	2.01
R_1[a)]/R_w[b)]	0.051/0.143	0.039/0.091
Reflections	3649 ($I < 2.0\sigma(I)$)	2211 ($I < 2.0\sigma(I)$)

a) $R_1 = \Sigma||F_0| - |F_c||/\Sigma|F_0|$. b) $R_w = [\Sigma w(|F_0| - |F_c|)^2/\Sigma wF_0^2]^{1/2}$.

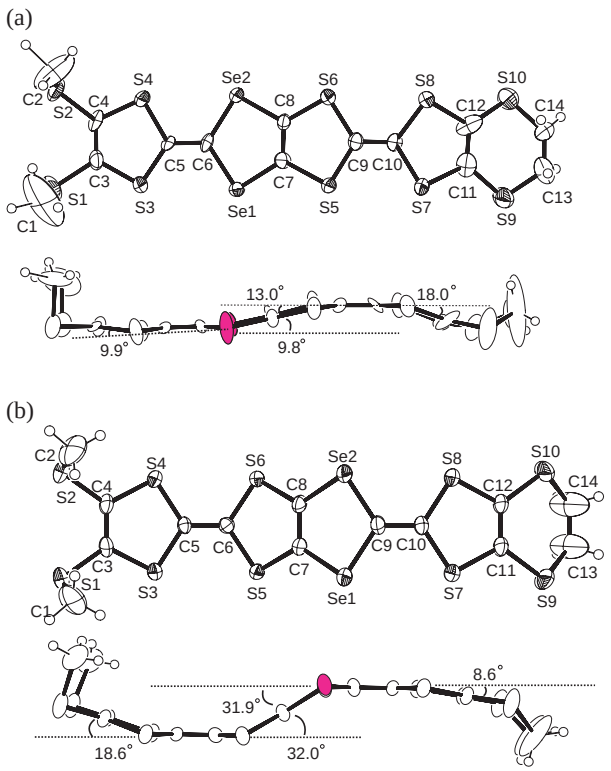

Figure 2. (a) ORTEP drawings of top and side views of the neutral crystal of **1**, and the atomic numbering scheme. (b) ORTEP drawings of top and side views of the neutral crystal of **2**, and the atomic numbering scheme.

Crystal Structures of Neutral Crystals. X-ray single crystal structure analyses have been performed for neutral crystals of **1** and **2**. The crystallographic data are shown in Table 2. The molecular structures of **1** and **2** are shown in Figure 2. The terminal methylthio groups of both **1** and **2** extend almost perpendicular to the molecular plane. The core π-skeleton is bent in an S-shape manner, and **2** has larger distortion. Similar clanked shape has been observed in other selenium-substituted neutral TMET-TTP derivatives and neutral

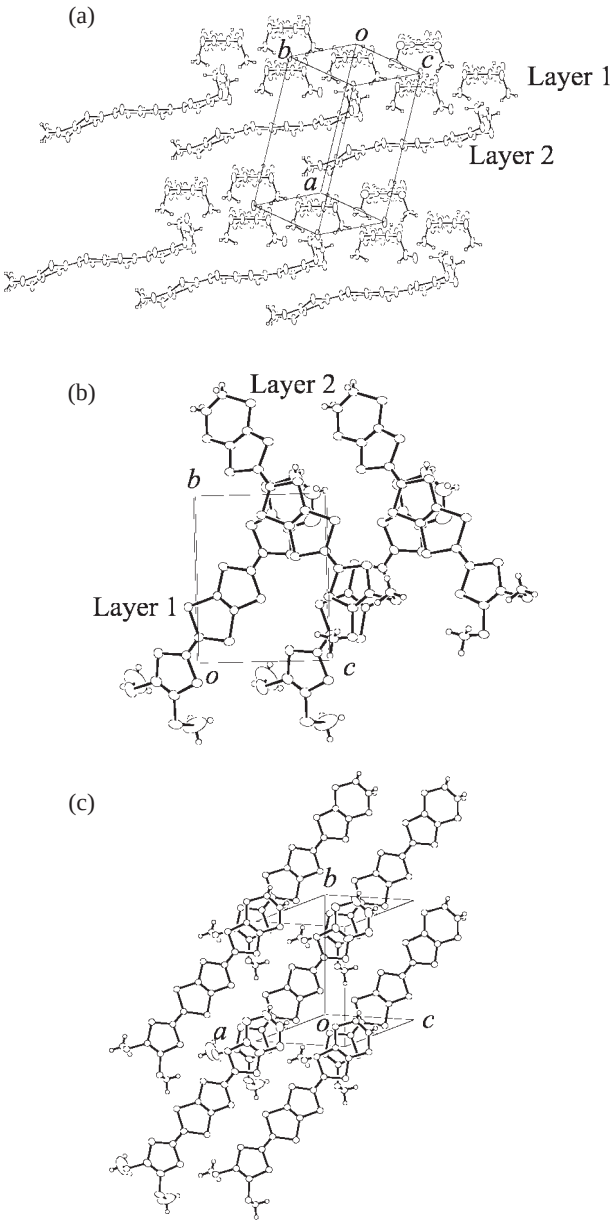

Figure 3. Crystal structures of neutral **1**, (a) projection along the molecular long axis ($b + c$) in Layer 1, and (b) view along the a axis. (c) Crystal structure of Layer 1 in the molecular stacking direction.

TTC_3-TTP.[12,13]

The crystal structures of **1** and **2** are shown in Figures 3 and 4. Despite the similarity of the molecular structures, **1** and **2** have quite different crystal structures. Compound **1** has one crystallographically independent donor molecule, and two molecules exist in a unit cell with the space group of $P2_1$. On the other hand, **2** has one crystallographically independent donor molecule, and four molecules exist in a unit cell with the space group $P2_12_12_1$. As for **2**, we have attempted to solve the crystal structure with the space group *Pnma* because the existence of a mirror plane perpendicular to the molecular plane is likely, but the analysis was unsuccessful. In the crystal structure of **1**, two molecular layers, designated as Layer 1 and Layer 2, are stacked alternately along the a axis (Figures 3a

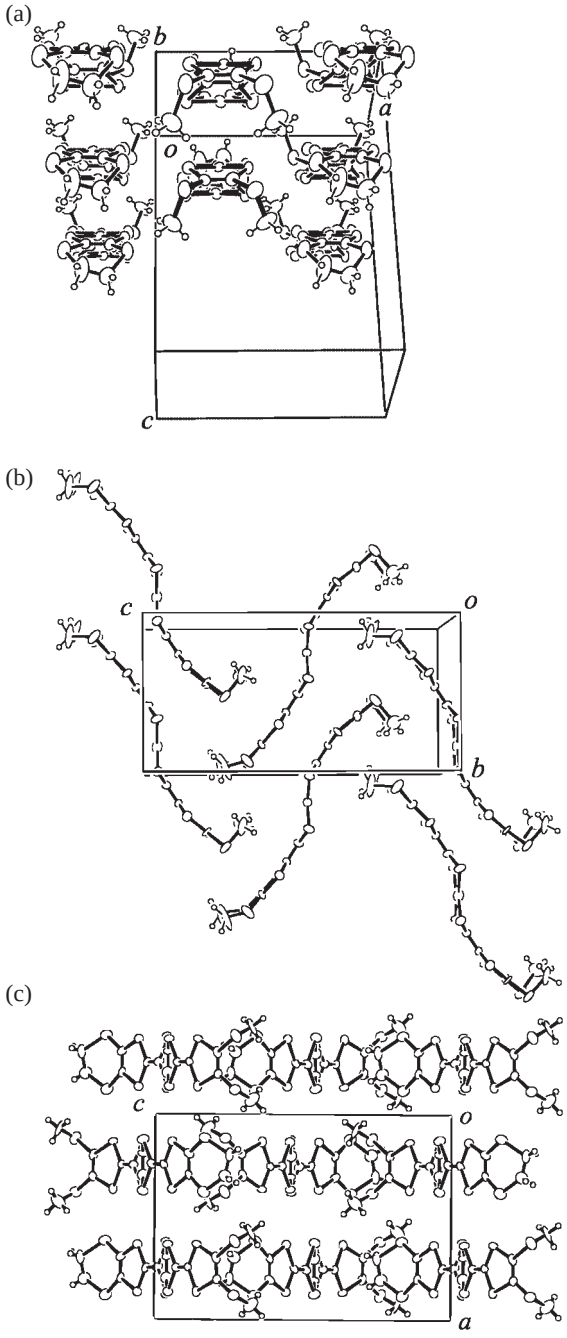

Figure 4. Crystal structures of neutral **2**, (a) projection along the molecular long axis, (b) projection along the molecular short axis, and (c) projection along the *b* axis.

and 3b). In Layer 1, the donor molecules are arranged parallel to $b + c$ corresponding to the molecular long axis, with a little overlap of the terminal units (Figure 3c). Layer 2 is generated from Layer 1 by the symmetry operation of 2_1, where the molecular long axis direction becomes $b - c$. Between the layers, the TTP skeleton of one layer comes onto the terminal unit of another layer (Figure 3b). In **2**, the donor molecules stack uniformly along the *b* axis (Figure 4a), and form a zigzag arrangement along the *c* axis (Figure 4b). The intercolumnar direction is parallel to the *a* axis (Figure 4c).

The amount of molecular distortion is explained from the combination of (1) the position of Se, and (2) the difference of ethylenedithio and methylthio parts. For both compounds, the distortion is smaller in the Se-substituted parts. In addition, neutral TTM-TTF (TTM-TTF: tetrakis(methylthio)-TTF) has larger distortion than neutral BEDT-TTF.[14] Similarly the non Se-substituted methylthio part in **2** has larger curvature than the ethylenedithio part in **1**. Consequently, **2** has larger distortion than **1**.

Crystal Structures of the Charge-Transfer Salts. Charge-transfer salts were prepared by electrochemical oxidation of the donors in the presence of tetrabutylammonium salts of various anions. The conditions are listed in Table 3. X-ray single crystal structure analyses of the four salts have been performed at room temperature. Crystallographic data of these salts are listed in Tables 4 and 5. Although TMET-TTP salts generally have a θ-type structure, salts with a relatively small ReO_4 anion have a space group $P2_1/a$, and other relatively large anions such as AuI_2^- and PF_6^- lead to $P2_1/n$.[4] The Se-substituted SMES-BDS-TTP and SMES-TTP afford $P2_1/n$ phases.[12] In the two types, the interlayer molecular arrangement is slightly different, though the intralayer donor arrangements are basically the same.[4,12] Among the present compounds, the space group of AsF_6 salts is $P2_1/n$, and the others are $P2_1/a$. Interestingly, the Se substitution to the outer rings prefers $P2_1/n$, whereas the present Se substitution to the inner ring leads to both $P2_1/a$ and $P2_1/n$ depending on the anion size. The inner Se substitution works as if the substitution reduced the effective anion size, or increased the effective donor size, whereas the outer Se substitution works in an opposite way. The *c* axes of the **2** salts are slightly longer than those of the **1** salts. One donor molecule and half an anion molecule are crystallographically independent; the donor exists in a general position, and the anion locates at an inversion center. However, owing to the anion deficiency estimated from population analysis, the ratio of the anion to the donor is about 0.30. This agrees with the results of energy dispersion spectroscopy

Table 3. Conditions of Electrochemical Crystal Growth

Donors	Anion	Solvent	Current/μA	Temperature/°C	Chemical composition[a)]	σ_{rt}/S cm^{-1}
1	PF_6	THF	0.2	50	0.30(X), 0.26(E), 0.35(P)	45
	AsF_6	THF	0.5	50	0.30(X), 0.25(E)	13
2	PF_6	THF	0.2	50	0.33(X), 0.29(E), 0.36(P)	16
	AsF_6	THF	0.3	40	0.30(X)	10

a) X is determined from the ratio of sulfur of the donor and the phosphorus of the anion by using the X-ray single crystal structure analysis, E is based on EDS measurement from the ratio of sulfur and fluorine, which includes the deviation of about ±0.1, and P is based on the EPMA measurement from the ratio of sulfur and the phosphorus.

Table 4. Crystallographic Data of TMET-DSDTP (**1**) Complexes

	(**1**)$(PF_6)_{0.30}$	(**1**)$(AsF_6)_{0.30}$
Chemical formula	$C_{12}H_{10}F_{1.80}S_{10}P_{0.30}Se_2$	$C_{12}H_{10}As_{0.30}F_{1.80}S_{10}Se_2$
Formula weight	700.24	713.43
Shape	Black plate	Black plate
Crystal system	Monoclinic	Monoclinic
Space group	$P2_1/a$	$P2_1/n$
a/Å	40.62(1)	40.70(2)
b/Å	11.159(3)	11.133(6)
c/Å	5.011(2)	4.999(2)
β/°	93.52(3)	93.63(3)
V/Å^3	2266(1)	2260(1)
Z	4	4
D_{calcd}/g cm^{-3}	2.052	2.096
R_1[a)]/R_W[b)]	0.066/0.174	0.077/0.148
Reflection used	2179 ($I > 2.0\sigma(I)$)	2062 ($I > 2.0\sigma(I)$)

a) $R_1 = \Sigma||F_0| - |F_c||/\Sigma|F_0|$. b) $R_w = [\Sigma w(|F_0| - |F_c|)^2/\Sigma wF_0^2]^{1/2}$.

Table 5. Crystallographic Data of TMET-DTDSP (**2**) Complexes

	(**2**)$(PF_6)_{0.33}$	(**2**)$(AsF_6)_{0.30}$
Chemical formula	$C_{12}H_{10}F_{1.98}S_{10}P_{0.33}Se_2$	$C_{12}H_{10}As_{0.30}F_{1.80}S_{10}Se_2$
Formula weight	704.59	713.43
Shape	Black plate	Black plate
Crystal system	Monoclinic	Monoclinic
Space group	$P2_1/a$	$P2_1/n$
a/Å	40.54(6)	40.70(2)
b/Å	11.12(1)	11.112(5)
c/Å	5.056(9)	5.047(2)
β/°	93.5(1)	93.60(5)
V/Å^3	2274(5)	2277(2)
Z	4	4
D_{calcd}/g cm^{-3}	2.057	2.080
R_1[a)]/R_W[b)]	0.055/0.136	0.083/0.198
Reflection used	3388 ($I > 2.0\sigma(I)$)	3282 ($I > 2.0\sigma(I)$)

a) $R_1 = \Sigma||F_0| - |F_c||/\Sigma|F_0|$. b) $R_w = [\Sigma w(|F_0| - |F_c|)^2/\Sigma wF_0^2]^{1/2}$.

(EDS), and of electron probe micro analysis (EPMA) (Table 3). These compositions are similar to the reported ratio of other TMET-TTP salts.[4,12] Hereafter, we use the compositions determined from X-ray population analyses.

The molecular structure of the donor of the charge-transfer salts is shown in Figure 5. The core π-skeleton is almost flat contrary to the neutral crystals. One of the terminal methylthio groups (C1) tilts from normal to the molecular plane, and the other one (C2) extends almost perpendicular to the molecular plane.

The θ-type structure of (**1**)$(PF_6)_{0.30}$ is depicted in Figure 6.[4,12] The conducting sheet spreads along the bc plane (Figure 6a), and the donor layer and the anion layer are alternately arrayed along the a axis (Figure 6b). Although the anions are located in the pocket surrounded by the methylthio units and the ethylenedithio units of the donors, the methylthio unit extends into the anion layer (Figure 6b). The donor molecules make a uniform stacking structure with a head-to-head arrangement along the c axis (Figure 6c). The overlap mode of the donors in the column is the ring-over-atom type, which agrees with the structure slipping both along the molecular long axis and along the molecular short axis (Figure 6d).[15] Dihedral

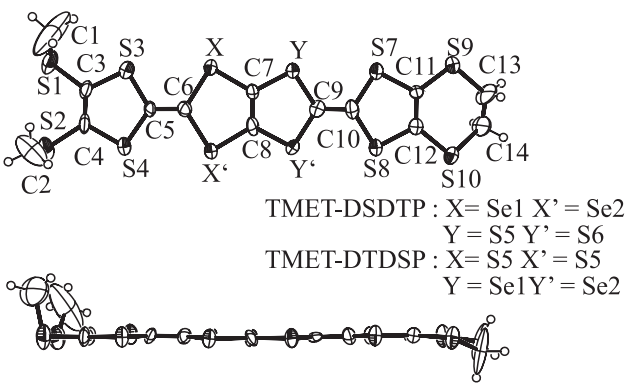

Figure 5. ORTEP drawings of top and side views of the donor molecule in the **1** and **2** salts, and the atomic numbering scheme.

angles (θ), slip distances (D_x and D_y) and interplaner distances (D_z) of these complexes are listed in Table 6, where D_x, D_y, and D_z are defined in Figure 6d. The AsF_6 salts have smaller dihedral angles than the PF_6 salts, and these are associated with the slightly large lattice constant c (Tables 4 and 5).

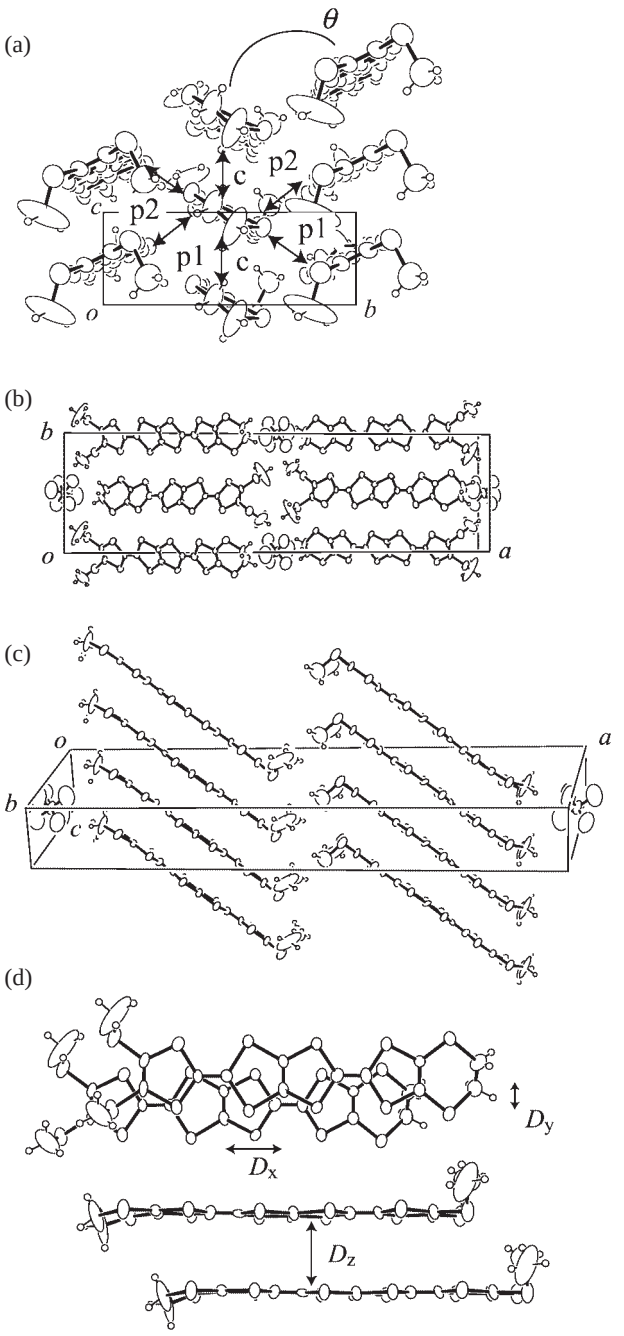

Figure 6. Crystal structure of (**1**)$(PF_6)_{0.30}$, (a) view along the molecular long axis, (b) projection along the c axis, and (c) view along the molecular short axis. (d) The overlap mode of the donor molecules in the salt.

Electronic Structures. The highest occupied molecular orbitals (HOMOs) of the donors in the obtained salts are calculated on the basis of the extended Hückel molecular orbital calculation (Figure 7). The sulfur 3d orbitals and the selenium 4d orbitals are not included because calculation without these orbitals provides appropriate shape of the Fermi surface in the TTP salts.[16] Close investigation of the HOMO indicates that the HOMO is more populated on the TTF part without Se atoms, which is indicated by shaded ovals in Figure 7. This HOMO unbalance is observed in the calculations of the AsF_6 salts as well as of the PF_6 salts (Figure 7). Such distribution reminds us of (TTM-TTP)I_3, which has an intramolecular CO such as TTF^+–TTF^0.[17] Since TMET-TTP is asymmetric, such an intramolecular CO is not essential as an origin of the MI transition. The HOMO distribution is, however, important to determine the difference of the conducting properties.

Table 6. Dihedral Angles and Slip Distances of TMET-DSDTP (**1**) and TMET-DTDSP (**2**) Complexes

	θ/deg	D_x/Å	D_y/Å	D_z/Å
(**1**)$(PF_6)_{0.30}$	125	3.01	1.75	3.60
(**1**)$(AsF_6)_{0.30}$	120	2.99	1.78	3.59
(**2**)$(PF_6)_{0.33}$	125	3.07	1.84	3.57
(**2**)$(AsF_6)_{0.30}$	120	3.04	1.80	3.61

Table 7. Calculated Intermolecular Overlap Integrals S_i ($\times 10^{-3}$)

	S_c[a)]	S_{p1}[a)]	S_{p2}[a)]
(**1**)$(PF_6)_{0.30}$	−3.64	1.63	2.03
(**1**)$(AsF_6)_{0.30}$	−3.54	1.64	1.95
(**2**)$(PF_6)_{0.33}$	−3.48	1.45	2.05
(**2**)$(AsF_6)_{0.30}$	−2.98	1.29	1.75
(TMET-TTP)$(PF_6)_{0.27}$[4]	−2.82	1.04	1.73

a) The overlap integrals are defined in Figure 6a.

The intermolecular overlap integrals S_i are estimated on the basis of the calculated HOMO (Table 7). As compared with the calculation of (TMET-TTP)$(PF_6)_{0.27}$,[4] the selenium substitution enhances the overlap integrals in all directions. The tight-binding band structures are calculated from the transfer integrals t_i estimated from $t_i = E \times S_i$, where E is the energy level of the HOMO (−10 eV) (Figure 8). The calculation affords a relatively isotropic closed Fermi surface. The Fermi surface previously reported for the TMET-TTP salts is more elongated along k_c,[4,12] but this is due to the overestimation of S_{p1} and S_{p2} coming from the sulfur 3d-orbitals.

Transport Properties. The temperature dependence of electrical resistivity is depicted in Figure 9. These salts show semiconducting properties down to liquid helium temperatures. In (**1**)$(PF_6)_{0.30}$, however, the resistivity becomes almost flat between about 200 and 50 K. Since the resistivity increases from room temperature to 200 K, this flat region is not a simple metallic state, but seems to be a highly conducting CO state. (**1**)$(AsF_6)_{0.30}$ has a similar flat region above 200 K. The charge localization temperature T_{CL} is defined by the temperature at which the resistivity starts to increase from the flat resistivity, because the TMET-TTP salts usually show weakly semiconducting behavior even at room temperature and do not show an obvious MI transition. For (**1**)$(PF_6)_{0.30}$, the charge localization takes place at $T_{CL} = 50$ K, while the corresponding temperature for (**1**)$(AsF_6)_{0.30}$ is $T_{CL} = 200$ K. The activation energy E_a is evaluated from the slope of the Arrhenius plot. The activation energies of the salts of **2** are about 70 meV (60 K $< T <$ 283 K). In **1**, E_a of the AsF_6 salt is 40 meV in the temperature region between 200 and 50 K, and E_a of the PF_6 salt is about 30 meV below 50 K.

The flat resistivity behavior seems to be associated with the enhanced HOMO population to the ethylenedithio-TTF part

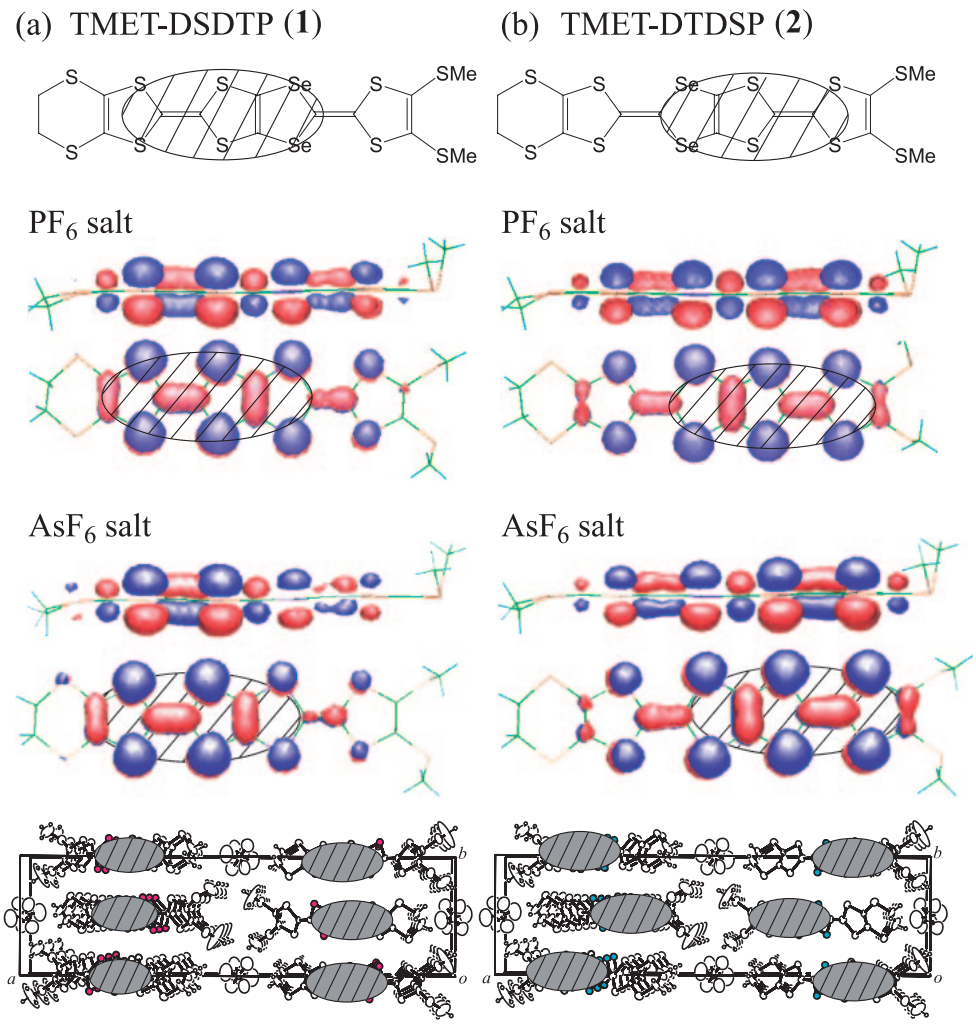

Figure 7. The HOMO shapes.

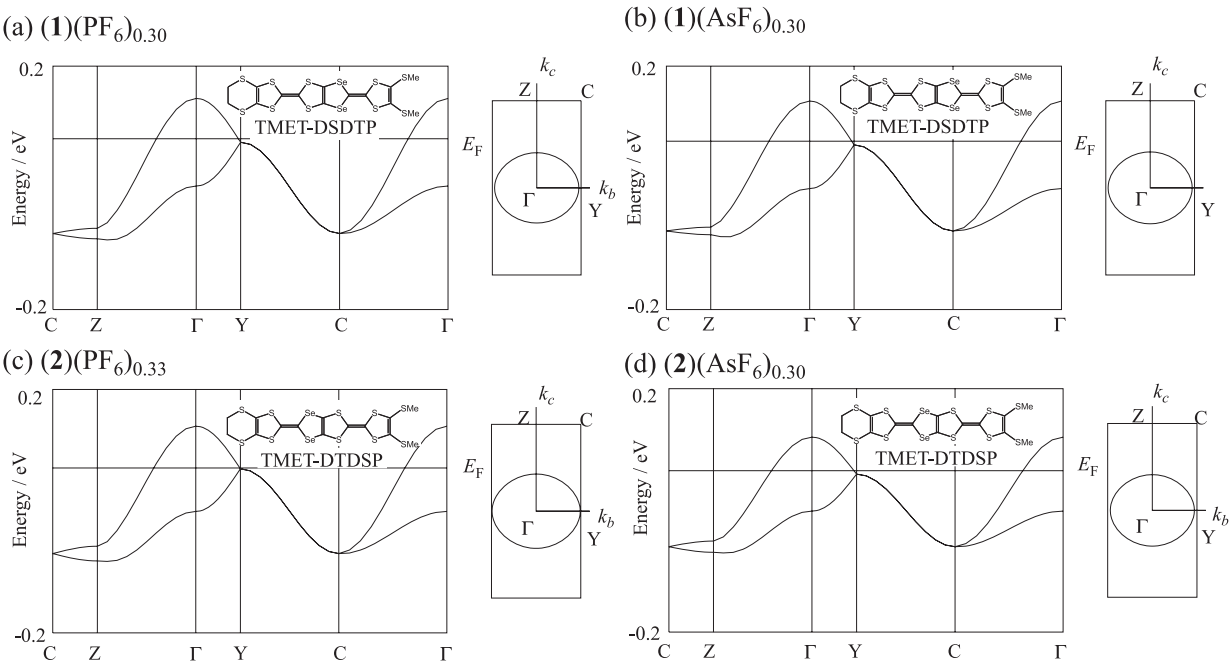

Figure 8. Band structures and the Fermi surfaces of (a) (**1**)$(PF_6)_{0.30}$, (b) (**1**)$(AsF_6)_{0.30}$, (c) (**2**)$(PF_6)_{0.33}$, and (d) (**2**)$(AsF_6)_{0.30}$.

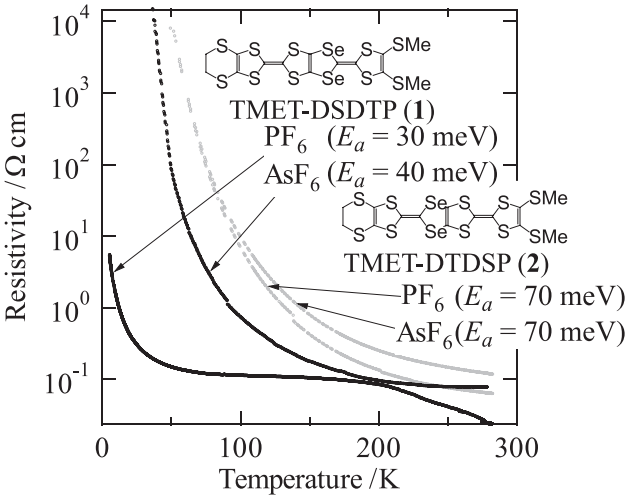

Figure 9. Temperature dependence of the resistivity of the PF_6 and AsF_6 salts of **1** and **2**.

(Figure 7). The large HOMO population at the ethylenedithio part increases the 2D character, and stabilizes the high conducting state. Furthermore, in the intercolumnar direction, the donors are slipped so as to avoid the bulky methylthio goups (Figure 6b), so that the ethylenedithio parts have more intercolumnar S–S contacts than the methylthio parts. Therefore, the HOMO shift to the ethylenedithio part is expected to enhance the intercolumnar interactions, p1 and p2. This is not clear in the actual calculation in Table 7, because the difference of the overlap integrals is smaller than the scatter coming from the different molecules. We also have to consider random potential of the anions because of the non-integer anion content. In order to determine the anion composition exactly, we have investigated the crystal structure of **1** by using synchrotron radiation at room temperature. However, we have not obtained any evidence of superstructure.

Since the present θ-phase salts have nearly 3:1 composition, the expected simplest CO is like $D^+D^0D^0$ in the extreme limit. Accordingly, the stripe phase with alternating D^+D^0 is impossible, and only the non stripe CO is possible. It is not surprising that the non stripe CO state leads to an insulating state at low temperatures because it loses charge carrier in the extreme limit, $D^+D^0D^0$. This seems to be consistent with the gradual MI transition, and the pressure dependence; the MI transition of the TMET-TTP salt is lowered by application of hydrostatic pressure as well as uniaxial strain in all directions.[18] We assume that the non stripe CO appears below 200 K in the salts of **1**. By contrast, the appearance of the non stripe CO does not solely establish the low-temperature insulating state, while the latter is potentially associated with other factors such as the HOMO unbalance investigated in the present work. This is the reason that the conducting behavior of **1** and **2** is so sensitive to the selenium substitution. We need, however, further experimental evidence to make the difference of $(\mathbf{1})(PF_6)_{0.30}$ and $(\mathbf{1})(AsF_6)_{0.30}$ clear.

Conclusion

We have synthesized **1** and **2**, in which S atoms of the inner TTP-skeleton are replaced by Se atoms. The Se substitution to the inner TTP-skeleton leads to flat resistivity over a wide temperature range. The Se substitution pushes the HOMO to the non Se-substituted part, and when this is the ethylenedithio part, the 2D interaction is enhanced to stabilize the high conducting state. This mechanism suggests the importance of charge redistribution in the double-TTF molecule. The insulating state of (TTM-TTP)I_3 has been attributed to the intramolecular CO, where the TTM-TTP molecule has a charge distribution such as TTF^+–TTF^0,[17] and the nonlinear conductivity of $(TSM\text{-}TTP)(I_3)_{5/3}$ has been interpreted by the intramolecular CO as well.[10b] The present work demonstrates potential control of intramolecular charge distribution in the double-TTF molecule by means of chemical modification such as Se substitution.

Experimental

General Data. All reactions were carried out under nitrogen atmosphere. Tetrahydrofuran (THF) was distilled over sodium–benzophenone before use. Trimethyl phosphite was distilled under nitrogen, and triethyl phosphite was distilled under reduced pressure. These phosphites were kept under nitrogen atmosphere. Cyclic voltammograms were measured on a Yanaco VMA-010 voltammogram. EDS and EPMA were measured at the Center for Advanced Materials Analysis, Tokyo Institute of Technology, with a JEOL JXA-8200 and EDAX DX-95, respectively. The melting points were determined with a Yanaco MP micro melting point apparatus. Mass spectra were obtained with a Shimadzu QP-5000 for EI-MS and a Shimadzu AXIMA-CFR for MALDI-TOF-MS. IR spectra were recorded on a SHIMADZU FTIR-8000 spectrometer. Microanalyses were performed at the Microanalytical Laboratory, Tokyo Institute of Technology.

4,5-Bis[2-(methoxycarbonyl)ethylthio]-1,3-diselenol-2-one (3) and 5-[4,5-Bis(methylthio)-1,3-dithiol-2-ylidene]-4,6-diselena-1,3-dithiapentalene-2-one (5a). Compounds **3** and **5a** were obtained by the same method as in Ref. 10.

5-[4,5-(Ethylenedithio)-1,3-dithiol-2-ylidene]-4,6-diselena-1,3-dithiapentalene-2-one (5b). 5b was synthesized by basically the same method as Ref. 10 (Scheme 2). 4,5-Ethylenedithio-1,3-dithiole-2-thione (**4b**) (1.9 g, 8.6 mmol) and **3** (1.3 g, 2.9 mmol) were heated in triethyl phosphite (10 mL) at 110 °C under nitrogen atmosphere for 3 h. After triethyl phosphite was evaporated in vacuo, the residue was chromatographed on silica gel with CH_2Cl_2. The resultant red oil and sodium methoxide (0.42 g, 7.7 mmol) were reacted in dry acetone (5.0 mL) and methanol (5.0 mL) under nitrogen atmosphere for 1 h. Anhydrous zinc chloride (0.044 g, 7.68 mmol) in 1.0-mL methanol and tetrabutylammonium bromide (0.21 g, 0.45 mmol) in 1.0-mL methanol were successively added. The formed precipitates were collected by filtration, washed with methanol, and dried in vacuo. The residue was suspended in distilled THF (5.0 mL), and cooled to −80 °C. Bis(trichloromethyl) carbonate (triphosgene, 0.13 g, 0.45 mmol) in distilled THF (3.0 mL) was slowly added dropwise to the suspension, and the resulting mixture was stirred for 2 h, and allowed to warm to room temperature for 5 h. The solvent was removed by rotary evaporator, and the residue was treated with methanol. The resulting precipitate was collected by filtration, and washed with water and methanol, and dried in vacuo. The product **5b** (0.42 g, 63%) was obtained as a green brown solid. No further purification was performed owing to the low solubility of **5b**.

5-[4,5-Bis(methylthio)-1,3-dithiol-2-ylidene]-2-(4,5-ethylenedithio-1,3-dithiol-2-ylidene)-4,6-diselena-1,3-dithiapentalene (TMET-DSDTP, 1). 5a (0.097 g, 0.21 mmol) and 4,5-ethylene-

dithio-1,3-dithiole-2-thione (**6a**) (0.16 g, 0.83 mmol) were reacted in trimethyl phosphite (3.0 mL) and toluene (6.0 mL) at 110 °C under nitrogen atmosphere for 2 h. The reacted mixture was cooled, and the resulting precipitate was collected by filtration. The residue was washed with methanol, and dried in vacuo. Chromatography (silica gel, CS_2) provided a red-orange solid of **1**. Recrystallization was carried out from the toluene solution, and afforded a shiny red-orange solid of **1** (0.053 g, 42%). Mp 254–255 °C; IR (KBr) 2910 (w), 2361 (w), 1457 (w) cm^{-1}; ^1H NMR (300 MHz, $CDCl_3$) 2.43 (s, 6H), 3.30 (s, 4H); MS(MALDI-TOF) m/z 655 (M^+); Anal. Calcd for $C_{14}H_{10}S_{10}Se_2$: C, 25.60; H, 1.53; S, 48.82%. Found: C, 25.59; H, 1.53; S, 48.76%.

2-[4,5-Bis(methylthio)-1,3-dithiol-2-ylidene]-5-(4,5-ethylenedithio-1,3-dithiol-2-ylidene)-4,6-diselena-1,3-dithiapentalene (TMET-DTDSP, 2). **5b** (0.10 g, 0.21 mmol) and 4,5-bis(methylthio)-1,3-dithiole-2-thione (**6b**) (0.19 g, 0.85 mmol) were reacted in trimethyl phosphite (5.0 mL) and toluene (8.0 mL) at 110 °C under nitrogen atmosphere for 3 h. The same procedure as TMET-DSDTP (**1**) afforded a shiny red solid of **2** (0.025 g, 18%). Mp 223–229 °C; IR (KBr) 2914 (w), 2352 (w), 1633 (w) cm^{-1}; ^1H NMR (300 MHz, $CDCl_3$) 2.42 (s, 6H), 3.31 (s, 4H); MS(MALDI-TOF) m/z 657 (M^+); Anal. Calcd for $C_{14}H_{10}S_{10}Se_2$: C, 25.60; H, 1.53%. Found: C, 24.91; H, 1.76%.

Single Crystal Grows of Neutral Crystals. Single crystals of **1** and **2** were grown by recrystallization from CS_2–hexane solutions (CS_2:hexane = 1:1 (vol.), 5 mL) with 1-mg donors.

Single Crystal X-ray Structure Analysis. Crystal structures of six compounds were determined by single-crystal X-ray diffraction. The data were measured by $\omega - 2\theta$ scan technique on a Rigaku automated four-circle diffractometer AFC-7R with graphite monochromatized Mo Kα radiation ($\lambda = 0.71069$ Å). All measurements were carried out at room temperature. The crystal structures were solved by direct method, SIR-92.[19] The structures were refined by full-matrix least-squares refinement by applying anisotropic temperature factors for all non-hydrogen atoms, in which isotropic temperature factors were applied to several atoms on account of relatively poor crystal quality. The hydrogen atoms were determined from the calculation. The anion population in the salts of **1a** and **1b** was estimated by population analysis. Crystalographic data have been deposited with Cambridge Crystallographic Data Centre: Deposition numbers CCDC 684771–684776. Copies of the data can be obtained free of charge via http://www.ccdc.cam.ac.uk/consts/retrieving.html (or from the Cambridge Crystallographic Data Centre, 12, Union Road, Cambridge, CB2 1EZ, UK; Fax: +44 1223 336033; e-mail: deposit@ccdc.cam.ac.uk).

Physical Properties. Electrical resistivity was measured for a single crystal by the four-probe method using a low-frequency ac current. Electrical contacts to the crystals were made with $\phi = 15$ µm gold wire and carbon paint. The transport measurement was performed along the crystal long axis, which corresponds to the donor stacking axis.

The authors thank Prof. Y. Misaki, Prof. K. Takimiya, and Prof. T. Otsubo for advice on the synthesis of **1** and **2**, and are obliged to Prof. H. Sawa and Dr. T. Kakiuchi for help with the synchrotron radiation X-ray. This work was partly supported by Grant-in-Aid for Scientific Research on Priority Areas of Molecular Conductors (No. 15073211) from MEXT.

References

1 T. Ishiguro, K. Yamaji, G. Saito, *Organic Superconductors*, 2nd ed., Springer, Berlin, **1998**.

2 Y. Misaki, H. Nishikawa, K. Kawakami, S. Koyanagi, T. Yamabe, M. Shiro, *Chem. Lett.* **1992**, 2321.

3 T. Mori, H. Inokuchi, Y. Misaki, T. Yamabe, H. Mori, S. Tanaka, *Bull. Chem. Soc. Jpn.* **1994**, *67*, 661.

4 Y. Misaki, H. Nishikawa, T. Yamabe, T. Mori, H. Inokuchi, H. Mori, S. Tanaka, *Chem. Lett.* **1993**, 729; T. Mori, H. Inokuchi, Y. Misaki, H. Nishikawa, T. Yamabe, H. Mori, S. Tanaka, *Chem. Lett.* **1993**, 733.

5 H. Mori, S. Tanaka, T. Mori, Y. Maruyama, *Bull. Chem. Soc. Jpn.* **1995**, *68*, 1136; H. Kobayashi, R. Kato, A. Kobayashi, Y. Nishio, K. Kajita, W. Sasaki, *Chem. Lett.* **1986**, 789; **1986**, 833.

6 H. Mori, S. Tanaka, T. Mori, *Phys. Rev. B* **1998**, *57*, 12023.

7 T. Mori, H. Mori, S. Tanaka, *Bull. Chem. Soc. Jpn.* **1999**, *72*, 179.

8 a) H. Seo, *J. Phys. Soc. Jpn.* **2000**, *69*, 805; T. Mori, *J. Phys. Soc. Jpn.* **2003**, *72*, 1469. b) M. Watanabe, Y. Noda, Y. Nogami, H. Mori, *Synth. Met.* **2003**, *135–136*, 665. c) R. Chiba, K. Hiraki, T. Takahashi, H. M. Yamamoto, T. Nakamura, *Phys. Rev. Lett.* **2004**, *93*, 216405.

9 Y. Misaki, T. Kochi, T. Yamabe, T. Mori, *Adv. Mater.* **1998**, *10*, 588.

10 a) M. Ashizawa, A. Akutsu, B. Noda, N. Nii, T. Kawamoto, T. Mori, T. Nakashiki, Y. Misaki, K. Takimiya, T. Otsubo, *Bull. Chem. Soc. Jpn.* **2004**, *77*, 1449. b) T. Mori, T. Kawamoto, I. Terasaki, T. Kakiuchi, H. Sawa, *Phys. Rev. B* **2007**, *75*, 235103.

11 T. Mori, M. Ashizawa, M. Aragaki, K. Murata, Y. Misaki, K. Tanaka, *Chem. Lett.* **1998**, 253.

12 M. Ashizawa, N. Nii, T. Mori, Y. Misaki, K. Tanaka, K. Takimiya, T. Otsubo, *Bull. Chem. Soc. Jpn.* **2003**, *76*, 2091.

13 S. Kimura, H. Kurai, T. Mori, *Tetrahedron* **2002**, *58*, 1119.

14 H. Kobayashi, A. Kobayashi, Y. Sasaki, G. Saito, H. Inokuchi, *Bull. Chem. Soc. Jpn.* **1986**, *59*, 301; C. Katayama, M. Honda, H. Kumagai, J. Tanaka, G. Saito, H. Inokuchi, *Bull. Chem. Soc. Jpn.* **1985**, *58*, 2272.

15 T. Mori, *Bull. Chem. Soc. Jpn.* **1998**, *71*, 2509.

16 J. Ouyang, K. Yakushi, Y. Misaki, K. Tanaka, *J. Phys. Soc. Jpn.* **1998**, *67*, 3191; T. Kawamoto, M. Ashizawa, T. Mori, T. Yamamoto, J. Yamaura, H. Tajima, *J. Phys. Soc. Jpn.* **2002**, *71*, 3059; O. Drozdova, K. Yakushi, Y. Misaki, K. Tanaka, *J. Solid State Commun.* **2002**, *168*, 497.

17 Y. Nogami, T. Kambe, N. Fujimura, K. Oshima, T. Mori, T. Kawamoto, *Synth. Met.* **2003**, *135–136*, 637; R. Swietlik, K. Yakushi, K. Yamamoto, T. Kawamoto, T. Mori, *Synth. Met.* **2005**, *150*, 83.

18 T. Takeuchi, H. Hoshino, R. Kondo, S. Kagoshima, M. Enomoto, T. Kawamoto, T. Mori, *J. Phys. Soc. Jpn.* **2003**, *72*, 1152.

19 A. Altomare, G. Cascarano, C. Giacovazzo, A. Guagliardi, *J. Appl. Crystallogr.* **1993**, *26*, 343.